The Astronomical Journal, 166:247 (8pp), 2023 December https://doi.org/10.3847/1538-3881/ad03f3

A Lithium Depletion Age for the Carina Association

Mackenna L. Wood[1,2], Andrew W. Mann[1], Madyson G. Barber[1], Jonathan L. Bush[1], Reilly P. Milburn[1], Pa Chia Thao[1,5], Stephen P. Schmidt[3], Benjamin M. Tofflemire[4,6], and Adam L. Kraus[4]
[1] Department of Physics and Astronomy, The University of North Carolina at Chapel Hill, Chapel Hill, NC 27599, USA; woodml@mit.edu
[2] MIT Kavli Institute for Astrophysics and Space Research Massachusetts Institute of Technology, Cambridge, MA 02139, USA
[3] Department of Physics and Astronomy, Johns Hopkins University, Baltimore, MD 21218, USA
[4] Department of Astronomy, The University of Texas at Austin, Austin, TX 78712, USA
Received 2023 June 23; revised 2023 October 3; accepted 2023 October 11; published 2023 November 15

Abstract

The dispersed remnants of stellar nurseries, stellar associations, provide unparalleled samples of coeval stars critical for studies of stellar and planetary formation and evolution. The Carina Stellar Association is one of the closest stellar associations to Earth, and yet measurements of its age have varied from 13 to 45 Myr. We aim to update the age of Carina using the lithium depletion boundary (LDB) method. We obtain new measurements of the Li 6708 Å absorption feature in likely members using optical spectra from the Goodman High Throughput Spectrograph on SOAR and NRES on LCO. We detect the depletion boundary at $M_K \simeq 6.8$ (M5). This age is consistent within uncertainties across six different models, including those that account for magnetic fields and spots. We also estimate the age through analysis of the group's overall variability, and by comparing the association members' color–magnitude diagram to stellar evolutionary models using a Gaussian Mixture Model, recovering ages consistent with the LDB. Combining these age measures we obtain an age for the Carina association of 41^{+3}_{-5} Myr. The resulting age agrees with the older end of previous age measurements and is consistent with the lithium depletion age for the neighboring Tucana-Horologium moving group.

Unified Astronomy Thesaurus concepts: M dwarf stars (982); Stellar associations (1582)

1. Introduction

Young stellar associations are valuable tools for studying stellar and planetary evolution. It is thought that all or nearly all stars form in associations with tens or hundreds of other stars as giant molecular clouds collapse, triggering star formation. These groups of coeval stars spread out over the first Gyr after their formation, dispersing until they are indistinguishable from the rest of the field. Prior to their full dispersal, young associations can serve as stellar laboratories, each providing a sample of stars with the same initial environmental conditions, age, and kinematic trajectory across a range of stellar types. Young coeval populations have facilitated the study of stellar evolutionary paths (e.g., Bell et al. 2013), protoplanetary disks and planet formation (e.g., Fang et al. 2013), and young planet evolution (e.g., Ciardi et al. 2018; Bohn et al. 2020; Bouma et al. 2022; Mann et al. 2022).

The Carina Association is one such young association. Discovered by Torres et al. (2001), it was originally considered part of the Great Austral Young Association (GAYA) complex, which included two additional nearby associations, Tucana-Horologium and Columba. However, the relationships between these groups is uncertain. Tucana-Horologium may be independent from Carina-Columba (Kraus et al. 2014), or it may be part of the larger complex. Gagné et al. (2021) used expanded kinematic information from Gaia Data Release 3 (DR3) to search for connections between populations, finding that Carina and Columba are connected through the Theia 92 and 113 groups (Kounkel et al. 2019) to Platais 8 (Platais et al. 1998). Additional evidence for a large complex in the region came from Kerr et al. (2022), which examined the connection between Carina, Columba, Tuc-Hor, Platais 8, and the Fornax-Horlogium association, finding that they can be linked as a single-star formation event with two "cores."

The relationships between these groups are further complicated by uncertainty in their ages. The three groups originally thought to form the GAYA complex were estimated to be about 40 Myr old. Tucana-Horologium, the largest and best studied of the three, was confirmed to be 40 Myr by Kraus et al. (2014). However, the ages of Carina and Columba are less certain. The age of Carina has been measured several times using a variety of membership lists and methods, resulting in estimates of 13 Myr (isochrone; Booth et al. 2021), ∼21 Myr (lithium sequence; Schneider et al. 2019), >28 Myr (kinematic; Miret-Roig et al. 2018), and 45^{+11}_{-7} Myr (isochrone; Bell et al. 2015).

A tighter age constraint on the Carina association will help to determine its relationship with nearby associations, but it can also provide constraints on the formation and evolution of planets. Members of Carina host debris (Moór et al. 2016) and protoplanetary disks (Silverberg et al. 2016; Murphy et al. 2018), are dippers (Gaidos et al. 2022), and have been suggested as an origin of the interstellar object 'Oumuamua (Hsieh et al. 2021). At a mean distance of 75 pc, Carina is also one of the closest known stellar associations, facilitating observational studies of such objects, including direct imaging and atmospheric characterization of planets.

A precise and fairly model-independent method for determining association age, the lithium depletion boundary (LDB) method relies on locating the sharp cutoff between Li-rich and Li-poor late-M dwarfs within the association. Lithium is depleted via proton–proton reactions in the cores of stars with

[5] NSF GRFP Fellow.
[6] 51 Pegasi b Fellow.

core temperatures $>2.5 \times 10^6$ K. As they approach the main sequence (MS), stars of different masses will reach this threshold temperature at different times. This results in a sharp boundary between those that have reached the threshold temperature and fully depleted their initial Li, and those slightly lower mass stars that have not and retain their full initial amount of Li. In fully convective late-M objects, this depletion is rapid and complete, leading to a very sharp depletion boundary, the age-dependence of which is not strongly effected by model choice or initial Li abundance (Burke et al. 2004; Tognelli et al. 2015). By focusing on these very-low-mass objects, LDB is less model dependent than methods using the Li abundances of early-M or higher-mass stars. In those partially convective stars, the depletion boundary is not as well defined and depends on factors such as convective overshoot, such that uncertainty in measurements or model choice causes more age uncertainty.

In this paper, we apply the LDB method, combined with an isochrone fit, empirical Li sequence comparison, and analysis of the group's variability, to measure the age of the Carina association. In Section 2, we describe our selection of Carina members using BANYAN Σ and color–magnitude diagram (CMD) information. Our observational program is described in Section 3, and in Section 4, we determine the age of the association. We conclude in Section 5 with a discussion and summary of our results.

2. Membership Selection

To select the initial list of Carina members we use the BANYAN Σ Bayesian tool for determining membership probabilities. BANYAN Σ uses kinematic models of nearby young associations to calculate the probability of a given star's membership within each association or the field. We use the kinematic models defined by Gagné et al. (2018) for most of the associations, but due to the proximity of Carina to Lower Centaurus Crux (LCC), and MELANGE-4 (Wood et al. 2023), we use an updated model for those groups. The new model of LCC, incorporating its subpopulations, and the model of MELANGE-4 are described in Mann et al. (2022) and Wood et al. (2023), respectively.

To construct the input sample for BANYAN Σ, we select from Gaia DR3 all stars within 100 pc of HD 49855, a high-probability member of Carina (Gagné et al. 2018). This sample comprised 542,642 stars. We use this selected sample rather than the full Gaia DR3 200 pc sample to decrease the computation time and memory demands from the BANYAN Σ run, and to ensure that we included all stars near the Carina association. We use Gaia DR3 RA, Dec, parallax, proper motion, and, when available, radial velocity.

From the results of BANYAN Σ, we take stars with membership probability $P > 50\%$ and for which Carina is the best hypothesis (BESTHYP = CAR), yielding 129 candidate members.

As BANYAN Σ only uses kinematic indicators of membership in determining the probability, the sample will include some older comoving interlopers. To remove them we use the empirical definition of the MS given by Pecaut et al. (2012), removing candidates that have $B_P - R_P > 1$, $G - R_P > 0.5$, and are fainter than the MS (see Figure 1). These cuts leave a membership list of 99 probable Carina members, shown in Figure 1.

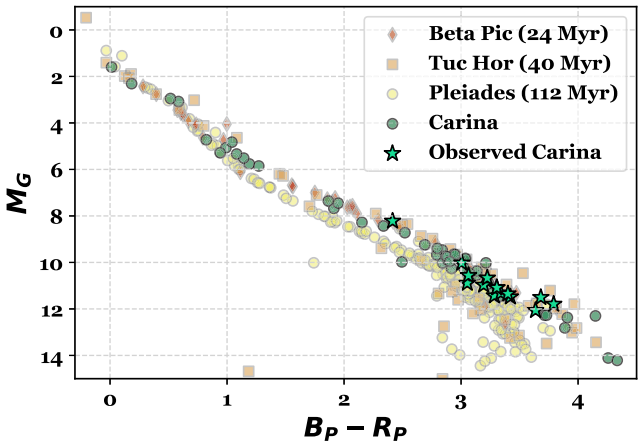

Figure 1. CMD of Carina members, overplotted with members of three benchmark associations, β Pictoris (24 Myr), Tuc-Hor (40 Myr), and Pleiades (112 Myr). Membership lists for benchmark associations are generated using BANYAN Σ with the same parameters as described in Section 2. High-probability members with RUWE < 1.2 are shown for benchmark associations. Observed members of Carina (see Table 1) are indicated with stars.

3. Observations

3.1. SOAR/Goodman

To obtain the medium-resolution optical spectra necessary for measuring the Li 6708 Å line in low-mass association members, we use the Goodman High Throughput Spectrograph (HTS) on the 4.1 m Southern Astrophysical Research Telescope (SOAR) located in Cerro Pachon, Chile. We observe a total of 15 candidate members of Carina. Observations were taken under mostly photometric conditions over five nights from 2020 February 6 through 2022 February 20.

These 15 stars were selected from the sample of candidate association members to map the LDB. We use an age estimate of 45 Myr (Bell et al. 2015) to predict the magnitude of the LDB. Comparing this age to BHAC 15 stellar evolutionary models (Baraffe et al. 2015), we calculate the expected Two-Micron All-sky survey (2MASS) K_S magnitude of 99% Li depletion. Stars with $\Delta K_S < 1$ of this predicted boundary are selected for observation. We update the observing list as needed as we obtain more data and revise the age estimate. Stars are prioritized for observation based on their Gaia RP magnitude and location on the sky. We omit potential binaries, as their inclusion could bias the measurement of age. We do so using the Gaia Renormalized Unit Weight Error (RUWE), a measure of the astrometric model goodness of fit. A high RUWE is indicative of binarity (Belokurov et al. 2020; Sullivan & Kraus 2021; Wood et al. 2021), so we remove those with RUWE > 1.2 from the observing list.

To measure the EW of the Li 6708 Å line, we use the Goodman red camera, 1200 l mm^{-1} grating, and the M5 mode, providing a wavelength coverage of 6300–7400 Å. We varied the slit width used between the 0.″45 slit and the 0.″6 slit depending on the target magnitude and the atmospheric seeing. This setup should give a resolving power of $R = 4500$–5800, although in practice the true resolution is lower and varies with exposure time (see below). For each target, we take five spectra with exposure times varying from 100 to 1600 s each.

To reduce the spectra we perform standard bias subtraction, flat-fielding, and optimal extraction of the target spectrum. Issues with the mount model and flexure compensation system

cause large wavelength shifts during and between exposures, with shifts up to 5–10 pixels between subsequent exposures. Following Wood et al. (2023), we correct this effect using simultaneous skyline spectra and Ne arc spectra taken prior to each image. For a majority of targets we use the simultaneous skyline spectra to determine a fourth-order polynomial wavelength solution, which is applied to calibrate each individual exposure. We then stack all exposures using a weighted mean. However, for targets with exposure times $t \lesssim 300$ s, the simultaneous skyline spectra do not have a sufficient signal-to-noise ratio (S/N) to determine the wavelength solution, so we use a fourth-order polynomial wavelength solution derived from the Ne arc and corrected with a linear factor based on the simultaneous telluric absorption lines. Each star is then corrected to its rest wavelength using radial-velocity standards taken with the same setup. While the resulting spectra were useful for determining spectral type and measuring EW(Li), we found that measured RVs had $\sigma_{\rm rv} \simeq 5$–10 km s^{-1}, based on spectra of RV standard stars. Therefore, we do not use these spectra to measure RV for membership confirmation.

3.2. LCO/NRES

To supplement our measurements of Li in low-mass association members we also obtain spectra of three higher-mass stars using the Network of Robotic Echelle Spectrographs (NRES; Siverd et al. 2018) at the Las Cumbres Observatory. Observations were taken between 2022 August 22 and 2022 September 9.

The NRES spectra cover a wavelength range of 380–860 nm with high resolution ($R \sim 53{,}000$). The data are reduced using the LCO NRES pipeline `BANZAI-NRES`.[7]

3.3. Measuring EW

Radial velocities are extracted by cross correlating the spectra with PHOENIX model atmospheres (Husser et al. 2013) for stars of the same spectral class. After correcting the spectrum to the star's rest frame, we measure the EW of the Li 6708 Å absorption line, used in Section 4.4.

We estimate the pseudocontinuum by fitting a line to the spectrum in the region on either side of the Li feature. This pseudocontinuum does not account for molecular contamination of the continuum, or the nearby Fe absorption feature (6707.4 Å), which should have minimal contribution in M dwarfs. The wavelength bounds of the line were adapted depending on the width of the line, which is effected by resolution differences between spectra and stellar $v \sin i_*$. We did not assume a Gaussian profile for the absorption feature, instead performing a trapezoidal sum of the line underneath the estimated pseudocontinuum. Doing so allows us to account for any distortion from a Gaussian profile caused by the slightly different wavelength solutions between the added exposures. Uncertainties were calculated by perturbing each point on the spectrum by its uncertainty (selected from a normal distribution) and recalculating the EW(Li). This process was repeated 500 times, and the resulting median and standard deviation were taken as the EW(Li) and the uncertainty. However, due to contamination of the continuum, the uncertainties for all targets are likely no better than 10%. An example of this is shown in Figure 2.

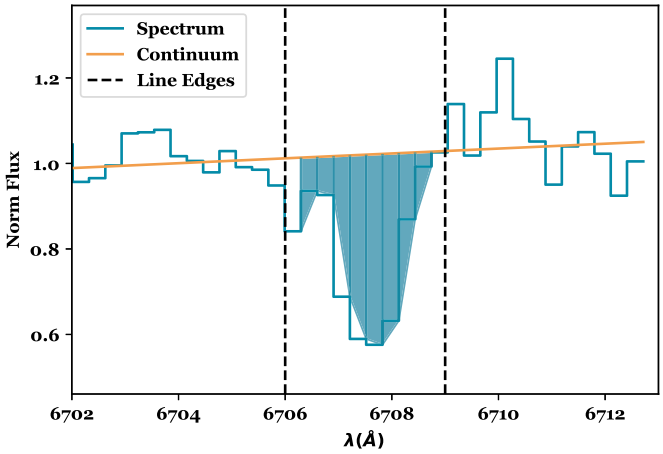

Figure 2. Example equivalent width measurement. The pseudocontinuum, shown in orange, is a linear fit of the spectrum in the regions on either side of the line edges. The EW is calculated using a trapezoidal sum between the spectrum and the pseudocontinuum fit.

Observations and resulting Li measurements are listed in Table 1. All SOAR/Goodman spectra are shown in Figure 3.

3.4. Archival

We obtain archival astrometry (α, δ, π, μ), photometry (B_P, R_P, and G), radial velocities, and Gaia RUWE for association members from Gaia DR3 (Gaia Collaboration et al. 2023).

We also obtain the J, H, and K_S magnitudes for all applicable members from the 2MASS (Skrutskie et al. 2006).

4. Revised Age of Carina

4.1. Isochrone

We first estimate the age of Carina by comparing Gaia photometry of stars in our updated membership list to two sets of isochrones: PARSECv1.2 (Bressan et al. 2012) and the Dartmouth Stellar Evolution Program (DSEP; Dotter et al. 2008) with magnetic enhancement (Feiden 2016). Both model grids have been shown to perform well on 10–150 Myr associations like Carina (e.g., Gillen et al. 2017; Mann et al. 2022; Wood et al. 2023).

For this comparison, we use a Gaussian-mixture model following Mann et al. (2022). To briefly summarize, the likelihood is formed from the mixture of two models as described in Hogg et al. (2010). The first model represents the single-star sequence of true members, and is described by two parameters: age (τ) and reddening ($E(B-V)$). The second model captures the outliers, which may include binaries, nonmembers, or stars with problematic photometry or parallaxes. The outlier model is described with two parameters: the offset from the first model (Y_B) and the variance around that offset (V_B). There are two additional free parameters, one to describe the amplitude of the outlier model (P_B), and one to handle underestimated uncertainties in the model and/or photometry (f). More details, including the likelihood function, can be found in the appendix of Mann et al. (2022).

We apply some quality cuts to the membership list from Section 2. Specifically, we remove stars with photometry outside the model grid, those with RUWE > 1.4, and those

[7] https://github.com/LCOGT/banzai-nres

Table 1
Observations of Carina Candidate Members

Object	Telescope	ObsDate (YYYYMMDD)	T_{exp} (s)	M_{K_s} (mag)	$B_P - R_P$ (mag)	G (mag)	EW(Li) (mÅ)
TIC 238236508	Goodman/SOAR	20200206	1500, 1600	7.18	3.421	15.777	529.5 ± 30.0
TIC 350559457	Goodman/SOAR	20200206	900	7.25	3.284	14.658	203.9 ± 19.5
TIC 167890419	Goodman/SOAR	20200305	600	7.22	3.791	16.362	646.9 ± 58.6
TIC 341935294	Goodman/SOAR	20200305	600	7.60	3.636	16.193	702.6 ± 36.3
TIC 167815117	Goodman/SOAR	20220218	900	7.15	3.339	15.922	618.0 ± 26.8
TIC 308085979	Goodman/SOAR	20220218	600	6.92	3.053	15.295	<10
TIC 308186410	Goodman/SOAR	20220218	700, 600	6.87	3.193	15.620	226.4 ± 25.2
TIC 349195685	Goodman/SOAR	20220218	600	6.60	3.064	15.307	<10
TIC 355794672	Goodman/SOAR	20220218	600	6.99	3.682	15.750	627.0 ± 28.0
TIC 384950919	Goodman/SOAR	20220218	180, 120	4.73	2.415	13.184	32.3 ± 19.2
Gaia 5258513835596515328	Goodman/SOAR	20220218	200	6.05	3.007	13.811	<10
TIC 302959739	Goodman/SOAR	20220219	750	6.87	3.305	15.630	377.6 ± 28.0
TIC 355373774	Goodman/SOAR	20220219	800	6.90	3.306	15.924	490.6 ± 34.2
TIC 452522881	Goodman/SOAR	20220219	300	6.54	3.224	15.087	<10
TIC 238714485	Goodman/SOAR	20220220	700	7.09	3.400	15.720	632.6 ± 22.2
HD 42270	NRES/LCO	20220905	1500	3.10	0.990	8.915	229.9 ± 11.3
HD 21024	NRES/LCO	20220822	600	2.14	0.585	5.406	<10
HD 44627	NRES/LCO	20220909	1200	3.48	1.082	8.838	183.2 ± 13.6

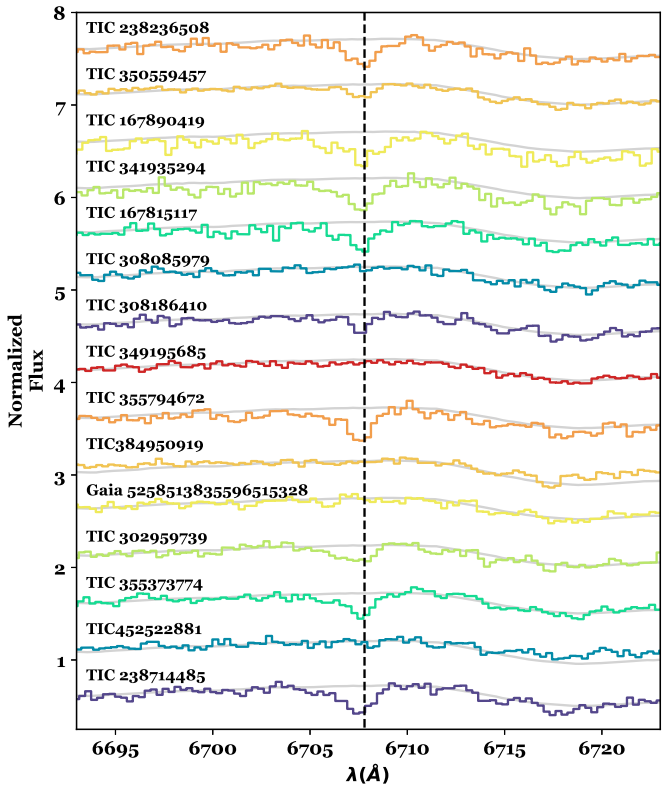

Figure 3. Reduced SOAR/Goodman spectra of all observed Carina members, overplotted with a Li-free M-dwarf template (gray; Bochanski et al. 2007). The wavelength of the Li 6707.8 Å line is marked with a vertical dashed line. Four of these stars show either no detectable Li, or have EW(Li) < 200 mÅ, and are thus Li-poor, while the other 11 have EW(Li) > 200 mÅ, and are Li-rich.

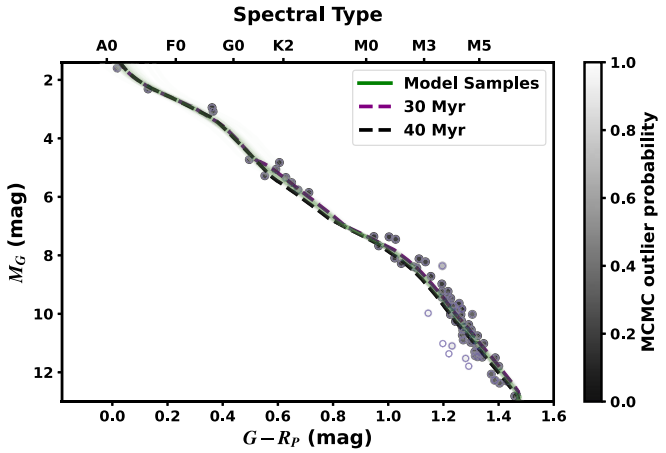

Figure 4. CMD of stars selected for fitting (blue circles) compared to PARSECv1.2 models. The green lines are 200 random samples from our MCMC analysis, and the two dashed lines are the 30 and 40 Myr isochrones for comparison. Points are shaded based on the probability that they are part of the main population or the outlier population.

with poor photometry or parallaxes (S/N of any absolute magnitude < 20).

We wrap the likelihood in a Markov chain Monte Carlo (MCMC) framework using `emcee` (Foreman-Mackey et al. 2013). The MCMC is run for 10,000 steps after an initial burn-in of 1000 steps, which far exceeds 50 times the autocorrelation time required for convergence. All parameters evolve under uniform priors with only physical limitations. Extinction is allowed to go negative to avoid Lucy–Sweeney bias (Lucy & Ricco 1979); we expect such nearby stars to have minimal reddening. To ensure uniform sampling in age, we resample the underlying model isochrones to increments of 0.1 Myr using the `isochrones` package (Morton 2015). We assume Solar metallicity but tested near-Solar metallicities ($-0.3 <$ [M/H] < 0.3). We show the Gaia CMD and model fit in Figure 4. The final fit yields an age of $\tau = 34 \pm 3$ Myr when using the PARSEC models, and $\tau = 39 \pm 3$ Myr when using the DSEP magnetic models. Different input assumptions, such as locking $E(B-V)$ to zero, changes in metallicity, or changing the assumed solar abundance scale, shift the resulting age at the $\simeq$3 Myr level, similar to the reported errors and the difference between the result of the two model grids.

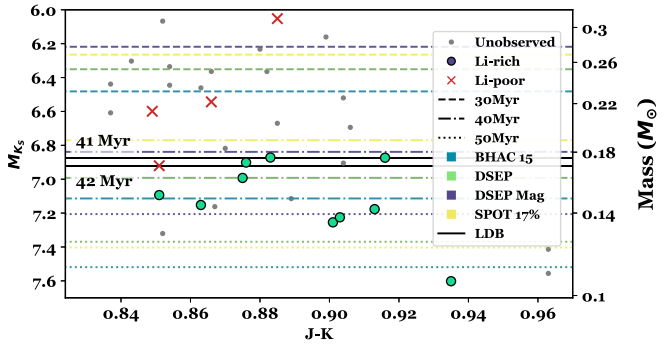

Figure 5. The lithium depletion boundary of Carina. Li-rich stars (EW (Li) > 200 mÅ) are shown as teal dots, and Li-poor (EW(Li) < 200 mÅ) ones as red x's. Black horizontal lines are drawn through the brightest Li-rich star and the faintest Li-poor one, and labeled with the corresponding age using the DSEP magnetic model. The LDB at 30, 40, and 50 Myr for each model is shown as colored lines, where the color indicates the model, and the line style indicates the age. The right side axis shows the stellar mass corresponding to the given magnitude at 40 Myr.

4.2. Variability

Barber & Mann (2023) present a method to estimate the age of a group from the overall variability of the members. While less precise, it is based purely on the variation in the Gaia photometry, and hence is independent of the other two methods. Using the combination of all three Gaia bands yielded an age estimate of 29^{+13}_{-7} Myr. This is within 1σ of our isochrone- and lithium-based estimates.

4.3. Lithium Depletion Boundary

We use the EW(Li) measurements obtained above to determine the association age in two ways: the LDB method, and by comparing the full Li sequence to benchmark associations.

The LDB method relies upon locating the sharp cutoff between Li-rich and Li-poor M dwarfs within the association, caused by the rapid depletion of Li in the cores of fully convective stars with core temperatures $>2.5 \times 10^6$ K. As they approach the MS, stars of different masses will reach this threshold temperature at different times, resulting in a sharp boundary between those which have reached it and fully depleted their initial Li, and those slightly lower mass stars which have not.

Identifying this boundary requires defining the threshold between Li-rich and Li-poor stars (see, e.g., Binks & Jeffries 2014; Binks et al. 2021). We use EW(Li) = 200 mÅ as the threshold (following Binks & Jeffries 2014). Using this threshold, we find that 12 of the observed stars are Li-rich (see Table 1 for Li measurements). The edges of the LDB are defined by the faintest Li-poor and brightest Li-rich stars. We find that the LDB is $6.87 < M_{K_s} < 6.92$, shown in Figure 5.

We determine the age of the association by comparing this magnitude range to stellar evolutionary models. We use six different models with varying treatments of convection, magnetic fields, and spots. For standard models we use the models from Baraffe et al. (2015; BHAC15) and Dotter et al. (2008; DSEP). For models with treatment of magnetic fields we use the Dotter models with magnetic enhancement from Feiden (2016; DSEP mag), and the stellar spot models from Somers et al. (2020) with 17% and 34% spot coverage (SPOT). The DSEP mag models are available based on stellar abundances from either Grevesse & Sauval (1998; GS98) or Asplund et al. (2009; AGSS09). We calculate the LDB age using both, but plot only the GS98 models on all figures.

Table 2
Upper and Lower Age Bounds given by each of the Models Used

Model	Lower Bound	Upper Bound
BHAC15	36 Myr	37 Myr
DSEP (GS98)	38 Myr	39 Myr
DSEP Mag (GS98)	41 Myr	42 Myr
DSEP Mag (AGSS09)	44 Myr	45 Myr
SPOT 17%	42 Myr	42 Myr
SPOT 34%	45 Myr	47 Myr

Note. The upper bound corresponds to the age given an LDB at the magnitude of the faintest observed Li-poor star, and the lower bound corresponds to the age given an LDB at the magnitude of the brightest observed Li-rich star.

For each model we calculate the magnitude corresponding to 99% Li depletion at each modeled age. We then linearly interpolate the resulting relationship between LDB magnitude and age to find the predicted age for the observed LDB. We repeat this interpolation using the top and bottom edges of the LDB to determine lower and upper age limits with each model, shown in Table 2. To calculate an overall age estimate we take the average of all estimates, resulting in an age of 41.5 ± 3.2 Myr.

A higher threshold of EW(Li) > 300 mÅ (as in Binks et al. 2021) results in three of the Li-rich stars becoming Li-poor, for a total of nine Li-rich stars. This changes the LDB bounds to be $6.87 < M_{K_s} < 7.25$, resulting in a slightly older age of 45.3 ± 5.7 Myr, which is still within the 2σ uncertainty bounds.

Another source of uncertainty in the LDB age measurement are the unobserved association members. There are several known members with magnitudes between the upper edge of the LDB and the next observed star. If some or all of these four stars are Li-rich, the top edge of the LDB would be shifted to a brighter magnitude, resulting in a younger age. The brightest unobserved star in this magnitude range is at $M_{K_s} = 6.608$. Using this as the lower age boundary results in an age of 38 ± 4 Myr, within the uncertainty bounds of our measurement.

4.4. Lithium Sequence

The Li sequence is an alternative method which utilizes Li measurements across a larger range of stellar masses. By comparing Li abundance as a function of color to either evolutionary models or benchmark associations, an age can be determined (Soderblom et al. 2014). When comparing to evolutionary models the dependence on initial Li abundance and greater reliance on factors such as convective overshoot make this method less robust to changes in model and less consistent than LDB. Using empirical comparison, the resulting age is only as model dependent as the age measurements of the benchmark association it is based on. Comparison of the Li sequence to models in particular often produces ages that are younger than those derived using the LDB.

To construct the Li sequence of Carina we use our Li measurements of low- and moderate-mass stars (see Table 1), supplemented with additional measurements from Riedel et al. (2017) and Schneider et al. (2019). We obtain 13 measurements from Riedel et al. (2017), and three from Schneider et al. (2019), listed in Table 3. Of the 13 in Riedel et al. (2017), they

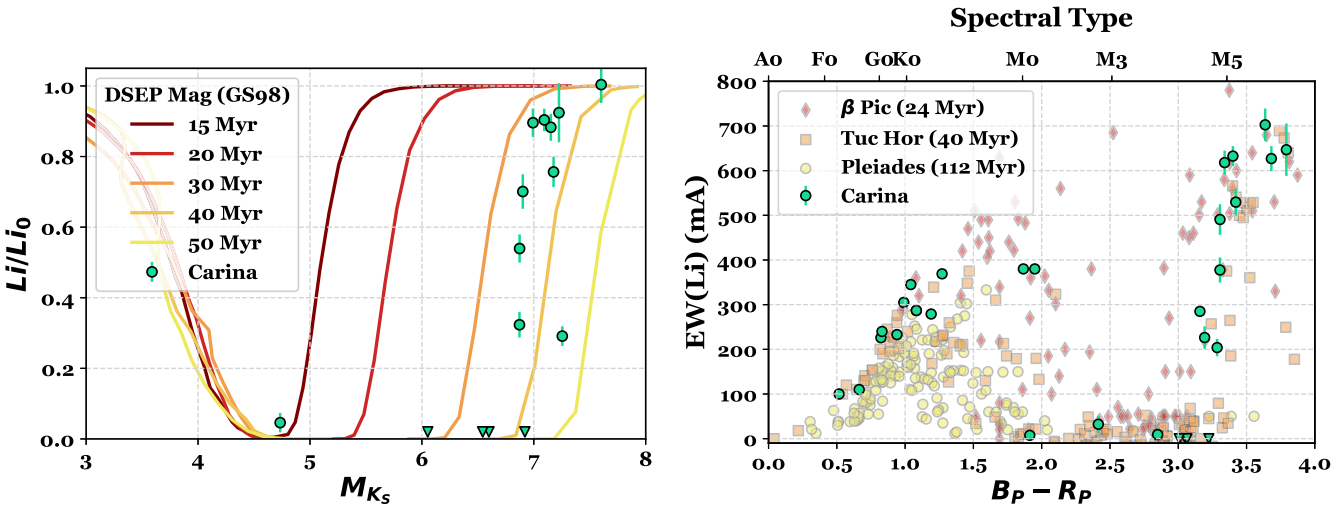

Figure 6. Lithium measurements of Carina members. (Left) Fraction of initial Li abundance as a function of Gaia $B_P - R_P$, overplotted with the DSEP magnetic models (Feiden 2016, DSEP mag). Equivalent widths of association members were converted to $\mathrm{Li/Li_0}$ using the curve of growth from Zapatero Osorio et al. (2002) for $T_{\rm eff} < 4000$ K and from Soderblom & Mayor (1993) for $T_{\rm eff} > 4000$ K. (Right) Lithium equivalent widths for Carina members, taken from our observations and Riedel et al. (2017), Schneider et al. (2019), are shown as teal dots plotted on top of the observed Li Sequences of the Beta Pictoris Moving Group (24 Myr, red; Binks & Jeffries 2014), Tucana-Horologium Young Association (40 Myr, orange; Kraus et al. 2014), and the Pleiades (112 Myr, yellow; Bouvier et al. 2018).

Table 3
Literature Li Measurements for Carina Members

Object	Gaia DR3	M_{K_s} (mag)	$B_P - R_P$ (mag)	G (mag)	EW(Li) (mA)	Source
HD 49855	5265670762922792960	3.561	0.940	8.995	233.0	Riedel et al. (2017)
TWA 21	5356713413789909632	3.569	1.271	9.477	369.0	Riedel et al. (2017)
HD 42270	4621305817457618176	3.096	0.990	8.915	305.0	Riedel et al. (2017)
AB Pic	5495052596695570816	3.48	1.082	8.838	287.0	Riedel et al. (2017)
HD 37402	4759444786175885824	2.828	0.664	8.267	110.0	Riedel et al. (2017)
2MASS J04082685-7844471	4625883599760005760	4.597	1.913	11.48	7.5	Riedel et al. (2017)
HD 55279	5208216951043609216	3.64	1.191	9.777	279.0	Riedel et al. (2017)
V0479 Car	5299141546145254528	3.043	1.041	9.747	345.0	Riedel et al. (2017)
2MASS J02564708-6343027	4721078629298085760	5.165	2.849	12.803	9.2	Riedel et al. (2017)
HD 269920	4658442922197295232	3.314	0.823	9.471	226.0	Riedel et al. (2017)
HD 83096[a]	5217846851839896704	1.71	0.516	7.413	100.0	Riedel et al. (2017)
HD 83096 B[a]	5217846851839896832	⋯	0.804	9.193	240.0	Riedel et al. (2017)
2MASS J07065772-5353463	5491506843495850240	4.314	1.866	10.71	380.0	Schneider et al. (2019)
2MASS J09032434-6348330	5297100607744079872	4.228	1.949	11.912	380.0	Schneider et al. (2019)
2MASS J09180165-5452332	5310606291358320512	5.127	3.159	13.15	285.0	Schneider et al. (2019)

Note.
[a] Binary, unresolved in 2MASS, but resolved in Gaia DR3.

classify eight as Carina members, while the remaining are either members of other nearby young associations (TW Hydrae and Tuc-Hor) or were not assigned membership in any association. We find that all have $P_{\rm BANYAN} > 60\%$.

To compare the observed stars against evolutionary models we first converted the measured EW(Li) to fraction of initial Li remaining, $\mathrm{Li/Li_0}$. To do so we determined initial Li abundance for each star using a curve of growth. The curve of growth for stars with $T_{\rm eff} < 4000$ K was taken from Zapatero Osorio et al. (2002) and that for stars with $T_{\rm eff} > 4000$ K from Soderblom & Mayor (1993). We then divided the EW(Li) by the initial EW(Li) to produce the Li fraction.

In Figure 6 we show both the empirical comparison of the Carina member Li measurements against benchmark associations and a comparison of the Li fraction to stellar evolutionary models.

Empirically, the Li sequence of Carina lies very near that of the Tuc-Hor association, shown in the right panel of Figure 6. The association has less Li at $B_P - R_P \simeq 3.0$ than the β Pic moving group (24 Myr), and does not transition to Li-rich stars until $B_P - R_P \simeq 3.25$. Kraus et al. (2014) found that Tuc-Hor has a LDB at $M_{K_s} = 7.12 \pm 0.16$. In that work they calculated an age of 41 ± 2 using that LDB and models from Baraffe et al. (1998). Using the method described in Section 4.3 with $M_{K_s} = 7.12 \pm 0.16$, we find an age for Tuc-Hor of 45.7 ± 4.7 Myr. This makes Tucana-Horologium slightly older than Carina, indicating that the empirical Li sequence of Carina is consistent with our calculated LDB age.

Comparing Li fraction against models shows that most of the points fall between the 30 and 40 Myr isochrones. This is somewhat younger than the previous estimates, but still consistent within the uncertainties.

5. Summary and Discussion

We measured the age of the Carina association using new Li measurements and the LDB method. Using Gaia DR3 kinematic measurements, and BANYAN Σ code with an updated list of associations, we created a new membership list of Carina, containing 99 stars. We obtained medium-resolution optical spectra of 15 low-mass association members using the Goodman HTS on the 4 m SOAR telescope, and supplemented these with spectra of K-type members taken with NRES on LCO. From these spectra we measured EW(Li), located the LDB, and constructed a Li sequence of the association. We supplemented the Li-based age measurements with a Gaussian-mixture model CMD fit, and analysis of the Gaia photometric variability. By combining all of the age measurements we obtain an age for the association of 41^{+3}_{-5} Myr. This includes estimates based on CMD position, photometric variability, LDB, and comparison of the Li sequence to benchmark associations and models.

Our age measurement is consistent with Bell et al. (2015). However, it is much older than the age found by Booth et al. (2021). That age was largely based on the inclusion of a single high-mass star, HD 95086, in the membership of Carina. Wood et al. (2023) found that that star is instead a high-probability member of the newly discovered MELANGE-4 association.

Our lithium-based age is also $\sim$2$\times$ the age found by Schneider et al. (2019) using a compilation of Li measurements. They found that the Li sequence of Carina more closely resembled the Li sequence of Beta Pic ($\sim$21 Myr) than that of Tuc-Hor ($\sim$40 Myr). Differentiation between those two ages comes largely from three stars with spectral type M0 and EW(Li) = 350–400 mÅ, which is higher than expected for a 40 Myr old star of that spectral type. Two of those three stars are included in the membership list we use here. Our age is based on Li measurements in fully convective low-mass stars, as there is less scatter in the Li levels for a single-aged populations in these stars than in warmer, partially radiative FGK and early-M dwarfs. New Li measurements in stars of type M3 and later make clear that the LDB for Carina, shown in Figures 5 and 6, is at a higher magnitude than that for β Pic. If Carina were the same age as β Pic, we would expect the three observed stars with $6.0 < M_{K_S} < 6.5$ to be Li-rich, and the partially depleted stars at $6.5 < M_{K_S} < 7.0$ not to be depleted at all. This discrepancy emphasizes the utility of the LDB method, which is less sensitive to model selection and which operates in a stellar regime with less star-to-star variation in lithium levels.

While we report a single age for Carina, not all members of an association form at the same time, leading to age spread within an association. However, this spread is difficult to disentangle from other factors, as any variation in an age-dependent property between members of an association may be caused by true age spread or by measurement error or age-unrelated variation in the property. Differences in stellar accretion history (Baraffe & Chabrier 2010; Baraffe et al. 2017), magnetic activity and spot fraction (e.g., Binks et al. 2021), extinction, circumstellar disks, binarity (Sullivan & Kraus 2021), and rotation may all appear as an age spread. It is possible that large age spreads are more common in stellar association complexes, such as Scorpius-Centaurus, where multiple formation events may have occurred over a $\sim$10 Myr period. Age spreads of 1–6 Myr have been measured in the Taurus complex (Krolikowski et al. 2021), and of 6–7 Myr within populations of Scorpius-Centaurus (Pecaut & Mamajek 2016). So an upper limit estimate of potential age spread within Carina would be $\pm$6 Myr.

While the LDB and Li sequence of the observed Carina members is very tight, there is one star with a lower than expected EW(Li) compared to its M_{K_s} (TIC 350559457). If the low Li is caused by age spread alone, based on the $\mathrm{Li}/\mathrm{Li}_0$ versus M_{K_s} sequence, this star would indicate age spread of 10 Myr (see Figure 6). However, its EW(Li) is very similar to other association members with a similar $B_P - R_P$ color. Additionally, none of the other observed stars differ by much from the expected Li for the determined age. The other methods we use are similarly consistent, with low CMD spread and a narrow LDB. Thus, it seems more likely that the low Li sequence position of TIC 350559457 is caused, at least in part, by measurement error or a different astrophysical reason than for it to be entirely from age spread.

The age we find here is consistent with the age of the nearby Tuc-Hor association (Kraus et al. 2014), lending support to the theory that the three groups form a complex as suggested early after their discovery (Torres et al. 2001) and by recent work (e.g., Kerr et al. 2021). Other potentially related groups include Theia 92, Theia 113, and Platais 8 (Gagné et al. 2021). Measuring LDB ages for those other groups to confirm their ages is an important next step to mapping out the larger star-forming complex.

If these groups, or a subset of them, are related, then this structure could be an older remnant of a Sco-Cen-like complex. Historically, older regions have been much harder to study because associations spread out as they age and galactic forces pull them apart. This has prevented the identification and study of older complexes—the only two well-studied complexes are both less than 20 Myr old. If so, this complex can reveal new insight into star formation and molecular cloud collapse mechanisms as well as to the stages of stellar and planetary evolution between 20 and 100 Myr.

Acknowledgments

A.W.M., M.G.B., and M.L.W. were supported by an NSF CAREER grant (AST-2143763). M.L.W., P.C.T., and R.P.M. were supported by the NC Space Grant Graduate Research program. P.C.T. was also supported by NSF Graduate Research Fellowship (DGE-1650116), the Zonta International Amelia Earhart Fellowship, and the Jack Kent Cooke Foundation Graduate Scholarship.

Many thanks to Patricio, Carlos, Juan, Sergio, and Rodrigo at SOAR for helping through many nights of observations.

This research includes data from observations obtained at the Southern Astrophysical Research (SOAR) telescope, which is a joint project of the Ministério da Ciência, Tecnologia e Inovações (MCTI/LNA) do Brasil, the US National Science Foundation's NOIRLab, the University of North Carolina at Chapel Hill (UNC), and Michigan State University (MSU).

This work has made use of data from the European Space Agency (ESA) mission Gaia (https://www.cosmos.esa.int/gaia), processed by the Gaia Data Processing and Analysis Consortium (DPAC; https://www.cosmos.esa.int/web/gaia/dpac/consortium). Funding for the DPAC has been provided by national institutions, in particular the institutions participating in the Gaia Multilateral Agreement.

This research has made use of the VizieR catalog access tool, CDS, Strasbourg, France. The original description of the

VizieR service was published in A&AS 143, 23. Resources supporting this work were provided by the NASA High-End Computing (HEC) Program through the NASA Advanced Supercomputing (NAS) Division at Ames Research Center for the production of the SPOC data products.

This work makes use of observations from the LCOGT NRES network.

Facilities: SOAR 4m (Goodman HTS), LCOGT 1m (NRES).

Software: Astropy (Astropy Collaboration et al. 2013, 2018), Astroquery (Ginsburg et al. 2019), matplotlib (Hunter 2007), BANYAN Σ (Malo et al. 2012; Gagné et al. 2018), BANZAI-NRES.

ORCID iDs

Mackenna L. Wood https://orcid.org/0000-0001-7336-7725
Andrew W. Mann https://orcid.org/0000-0003-3654-1602
Madyson G. Barber https://orcid.org/0000-0002-8399-472X
Jonathan L. Bush https://orcid.org/0000-0002-9446-9250
Reilly P. Milburn https://orcid.org/0000-0002-1312-3590
Pa Chia Thao https://orcid.org/0000-0001-5729-6576
Stephen P. Schmidt https://orcid.org/0000-0001-8510-7365
Benjamin M. Tofflemire https://orcid.org/0000-0003-2053-0749
Adam L. Kraus https://orcid.org/0000-0001-9811-568X

References

Asplund, M., Grevesse, N., Sauval, A. J., & Scott, P. 2009, ARA&A, 47, 481
Astropy Collaboration, Price-Whelan, A. M., Sipőcz, B. M., et al. 2018, AJ, 156, 123
Astropy Collaboration, Robitaille, T. P., Tollerud, E. J., et al. 2013, A&A, 558, A33
Baraffe, I., & Chabrier, G. 2010, A&A, 521, A44
Baraffe, I., Chabrier, G., Allard, F., & Hauschildt, P. H. 1998, A&A, 337, 403
Baraffe, I., Elbakyan, V. G., Vorobyov, E. I., & Chabrier, G. 2017, A&A, 597, A19
Baraffe, I., Homeier, D., Allard, F., & Chabrier, G. 2015, A&A, 577, A42
Barber, M. G., & Mann, A. W. 2023, ApJ, 953, 127
Bell, C. P. M., Mamajek, E. E., & Naylor, T. 2015, MNRAS, 454, 593
Bell, C. P. M., Naylor, T., Mayne, N. J., Jeffries, R. D., & Littlefair, S. P. 2013, MNRAS, 434, 806
Belokurov, V., Penoyre, Z., Oh, S., et al. 2020, MNRAS, 496, 1922
Binks, A. S., & Jeffries, R. D. 2014, MNRAS: Letters, 438, L11
Binks, A. S., Jeffries, R. D., Jackson, R. J., et al. 2021, MNRAS, 505, 1280
Bochanski, J. J., West, A. A., Hawley, S. L., & Covey, K. R. 2007, AJ, 133, 531
Bohn, A. J., Kenworthy, M. A., Ginski, C., et al. 2020, MNRAS, 492, 431
Booth, M., del Burgo, C., & Hambaryan, V. V. 2021, MNRAS, 500, 5552
Bouma, L. G., Kerr, R., Curtis, J. L., et al. 2022, AJ, 164, 215
Bouvier, J., Barrado, D., Moraux, E., et al. 2018, A&A, 613, A63
Bressan, A., Marigo, P., Girardi, L., et al. 2012, MNRAS, 427, 127
Burke, C. J., Pinsonneault, M. H., & Sills, A. 2004, ApJ, 604, 272
Ciardi, D. R., Crossfield, I. J. M., Feinstein, A. D., et al. 2018, AJ, 155, 10
Dotter, A., Chaboyer, B., Jevremović, D., et al. 2008, ApJS, 178, 89
Fang, M., Boekel, R. v., Bouwman, J., et al. 2013, A&A, 549, A15
Feiden, G. A. 2016, A&A, 593, A99
Foreman-Mackey, D., Hogg, D. W., Lang, D., & Goodman, J. 2013, PASP, 125, 306
Gagné, J., Faherty, J. K., Moranta, L., & Popinchalk, M. 2021, ApJL, 915, L29
Gagné, J., Mamajek, E. E., Malo, L., et al. 2018, ApJ, 856, 23
Gaia Collaboration, Vallenari, A., Brown, A. G. A., et al. 2023, A&A, 674, A1
Gaidos, E., Mann, A. W., Rojas-Ayala, B., et al. 2022, MNRAS, 514, 1386
Gillen, E., Hillenbrand, L. A., David, T. J., et al. 2017, ApJ, 849, 11
Ginsburg, A., Sipőcz, B. M., Brasseur, C. E., et al. 2019, AJ, 157, 98
Grevesse, N., & Sauval, A. 1998, SSRv, 85, 161
Hogg, D. W., Bovy, J., & Lang, D. 2010, arXiv:1008.4686
Hsieh, C.-H., Laughlin, G., & Arce, H. G. 2021, ApJ, 917, 20
Hunter, J. D. 2007, CSE, 9, 90
Husser, T.-O., von Berg, S. W., Dreizler, S., et al. 2013, A&A, 553, A6
Kerr, R., Kraus, A. L., Murphy, S. J., et al. 2022, ApJ, 941, 143
Kerr, R. M. P., Rizzuto, A. C., Kraus, A. L., & Offner, S. S. R. 2021, ApJ, 917, 23
Kounkel, M., Covey, K., Moe, M., et al. 2019, AJ, 157, 196
Kraus, A. L., Shkolnik, E. L., Allers, K. N., & Liu, M. C. 2014, AJ, 147, 146
Krolikowski, D. M., Kraus, A. L., & Rizzuto, A. C. 2021, AJ, 162, 110
Lucy, L. B., & Ricco, E. 1979, AJ, 84, 401
Malo, L., Doyon, R., Lafrenière, D., et al. 2012, ApJ, 762, 88
Mann, A. W., Wood, M. L., Schmidt, S. P., et al. 2022, AJ, 163, 156
Miret-Roig, N., Antoja, T., Romero-Gómez, M., & Figueras, F. 2018, A&A, 615, A51
Moór, A., Kóspál, Á., Ábrahám, P., et al. 2016, ApJ, 826, 123
Morton, T. D., 2015 isochrones: Stellar Model Grid Package, Astrophysics Source Code Library, ascl:1503.010
Murphy, S. J., Mamajek, E. E., & Bell, C. P. M. 2018, MNRAS, 476, 3290
Pecaut, M. J., & Mamajek, E. E. 2016, MNRAS, 461, 794
Pecaut, M. J., Mamajek, E. E., & Bubar, E. J. 2012, ApJ, 746, 154
Platais, I., Kozhurina-Platais, V., & Leeuwen, F. V. 1998, AJ, 116, 2423
Riedel, A. R., Blunt, S. C., Lambrides, E. L., et al. 2017, AJ, 153, 95
Schneider, A. C., Shkolnik, E. L., Allers, K. N., et al. 2019, AJ, 157, 234
Silverberg, S. M., Kuchner, M. J., Wisniewski, J. P., et al. 2016, ApJL, 830, L28
Siverd, R. J., Brown, T. M., Barnes, S., et al. 2018, Proc. SPIE, 10702, 107026C
Skrutskie, M. F., Cutri, R. M., Stiening, R., et al. 2006, AJ, 131, 1163
Soderblom, D. R., Hillenbrand, L. A., Jeffries, R. D., Mamajek, E. E., & Naylor, T. 2014, Ages of Young Stars (Tucson, AZ: Univ. Arizona Press)
Soderblom, D. R., & Mayor, M. 1993, AJ, 105, 226
Somers, G., Cao, L., & Pinsonneault, M. H. 2020, ApJ, 891, 29
Sullivan, K., & Kraus, A. 2021, ApJ, 912, 137
Tognelli, E., Prada Moroni, P. G., & Degl'Innocenti, S. 2015, MNRAS, 449, 3741
Torres, C. A. O., Quast, G. R., de La Reza, R., da Silva, L., & Melo, C. H. F. 2001, in ASP Conf. Ser. 244, Young Stars Near Earth: Progress and Prospects, ed. R. Jayawardhana & T. Greene (San Francisco, CA: ASP), 43
Wood, M. L., Mann, A. W., Barber, M. G., et al. 2023, AJ, 165, 85
Wood, M. L., Mann, A. W., & Kraus, A. L. 2021, AJ, 162, 128
Zapatero Osorio, M. R., Béjar, V. J. S., Pavlenko, Y., et al. 2002, A&A, 384, 937